Supporting Information (SI)

Excimer-Mediated Multiexciton Generation in Covalently Linked Cross Foldamers of Thiophene-Fused Perylene Bisimides

Weicong Li,[a] Wei Zhang,[b,c,*] Jiadong Zhou,[d] Linlin Liu,[a] Hongwei Song,[a,*] Zengqi Xie[a,*]

[a] State Key Laboratory of Luminescent Materials and Devices, Institute of Polymer Optoelectronic Materials and Devices, Guangdong Provincial Key Laboratory of Luminescence from Molecular Aggregates, Guangdong Basic Research Center of Excellence for Energy and Information Polymer Materials, South China University of Technology, Guangzhou 510640, P. R. China.

[b] Frontier Institute of Science and Technology, Xi'an Jiaotong University, Xi'an 710049, China.

[c] Institute of New Concept Sensors and Molecular Materials, Shaanxi Key Laboratory of New Conceptual Sensors and Molecular Materials, Xi'an Jiaotong University, Xi'an 710049, China

[d] School of Chemistry, South China Normal University, Guangzhou 510006, P. R. China.

ABSTRACT: Singlet fission (SF) is a promising strategy to surpass the Shockley-Queisser limit in organic photovoltaics, but the structural and electronic determinants controlling excimer-mediated multiexciton (ME) generation remain insufficiently understood. Herein, we designed two covalently linked cross foldamers, **CF(4)** and **CF(7)**, based on thiophene-fused perylene bisimide units, with controlled intramolecular chromophore rotational angles (88° and 55°) via alkyl chain engineering, while maintaining a constant π-π stacking distance. Steady-state and ultrafast spectroscopy studies revealed that both foldamers undergo excimer-mediated ME generation but with distinct dynamics: weakly coupled **CF(4)** (88°) achieves rapid ME formation in 27 ps, whereas strongly coupled **CF(7)** (55°) stabilizes the excimer, slowing ME formation to 114 ps. These results establish a clear structure–dynamics relationship, demonstrating that rotational angle modulation enables tuning of excimer energetics and SF efficiency, providing a general design strategy for π-conjugated assemblies.

Table of Contents

1. Materials and Methods

Materials. All solvents and reagents were purchased from commercial sources and used as received without further purification, unless otherwise stated.

Characterizations of compounds. ^{1}H NMR of $CDCl_3$ or $C_2D_2Cl_4$ solution was measured on a Bruker 400 MHz or 600 MHz NMR by using tetramethyl silane (TMS) as an internal standard. ^{13}C NMR spectra were not measured due to the poor solubility of the final products. At room temperature, the dimer exhibits broadened signals in the NMR spectrum due to concentration effects or rapid hydrogen exchange. Therefore, the measurement was conducted at an elevated temperature of 333 K in $C_2D_2Cl_4$ to obtain better-resolved NMR signals for target cross foldamers. Mass spectra were measured on a Waters ACQUITY TQD or MALDI-TOF spectrometer with α-cyano-4-hydroxycinnamic acid (CHCA) as MALDI matrices.

Optical characterizations. UV-vis absorption spectra were performed on a Shimadzu UV-3600 Plus spectrometer. Photoluminescence spectra were recorded on a Shimadzu RF-5301 spectrometer. All spectra were corrected for the characteristics of the lamp source and detection unit, respectively. Unless otherwise noted, dilute solutions of the materials were prepared in chloroform ($CHCl_3$) and toluene (TOL) as the solvent (10^{-5}~10^{-6} mol/L), if there is no special description.

MD simulations. All-atom MD simulations in this study were performed by using the MD program GROMACS. In the initial structure of the simulated system, the DFT-optimized structures of CF(4) and CF(7), as described below, were placed at the center of a cubic MD cell with dimensions 17.763 × 15.087 × 9.292 nm**.** The molecular topology and nonbonded parameters were generated by Sobtop, employing GAFF-like atom types. The atomic charges of both molecules were calculated using the restrained electrostatic potential (RESP)[3] methodology based on DFT calculations (*ω*B97XD/def2SVP) with the GAUSSIAN 16. Initial velocities were generated from a Maxwell distribution at 300 K. Production MD was carried out using the md integrator with a timestep of 1 ps for 2000 steps. Initial velocities were generated from a Maxwell distribution at 300 K. All bonds involving hydrogen atoms were constrained using the LINCS algorithm. Nonbonded interactions were treated with the Verlet cutoff scheme. Van der Waals interactions were handled using a cutoff with force-switching and long-range dispersion correction. Trajectory frames were saved every 2000 steps**.**

TA experiment. The fs-TA spectra were measured using a home-built femtosecond pump-probe setup. The laser pulse (800 nm, 35 fs pulse width, 1 kHz repetition rate) was generated by a regeneratively amplified Ti:sapphire laser (Coherent Astrella-Tunalbe-USP, USA). The output of the pulse is then divided into two beams with a beam splitter. For the pump beam, the TOPAS Prime (Light Conversion) was used to generate the pulse with a central wavelength locate at the 0-0 absorption band (500 nm). The probe beam was delayed with a computer-controlled optical delay line and then focused on a thin sapphire plate to generate the white light supercontinuum which split into two beams by using a broadband 50/50 beam splitter as the signal and reference beams. The focused pump and probe pulses were overlapped into a sample cuvette. The mutual polarization between the pump and probe beams was set to the magic angle (54.7°) by placing a

half-wave plate in the pump beam. No photodegradation was observed after the fs-TA experiments, as confirmed by the steady-state absorption spectra.

The ns-TA spectra were measured by a commercial spectrometer (Time-Tech Spectra). The generation of the pump beam is the same as that in fs-TA. The probe beam was generated from a supercontinuum laser (LEUKOS-DISCO, French) with the spectral region from 350 nm to 1800 nm, the repetition rate is 2 kHz, pulse width is 700 ps - 1 ns. No photodegradation was observed after the ns-TA experiments, as confirmed by the steady-state absorption spectra.

Transient absorption spectra of Ref, CF(4) and CF(7) were recorded in dilute TOL and CHCl3 at 10^{-5} M to avoid intermolecular interaction.

TRPL. Time-resolved photoluminescence (TRPL) was measured using a time-correlated single photon counting (TCSPC) system (FluoTime 300, PicoQuant, Germany). Excitation was provided at 375 nm. Emission decays were collected at representative wavelengths corresponding to the monomer (530 nm) and excimer emission (510 nm or 650 nm), and fitted with mono- or di-exponential analysis to extract lifetimes τ. Radiative and nonradiative rates were estimated from τ and PLQY using $k_r = \Phi/\tau$ and $k_{nr} = (1-\Phi)/\tau$. All TRPL experiments were performed at room temperature.

2. Synthesis

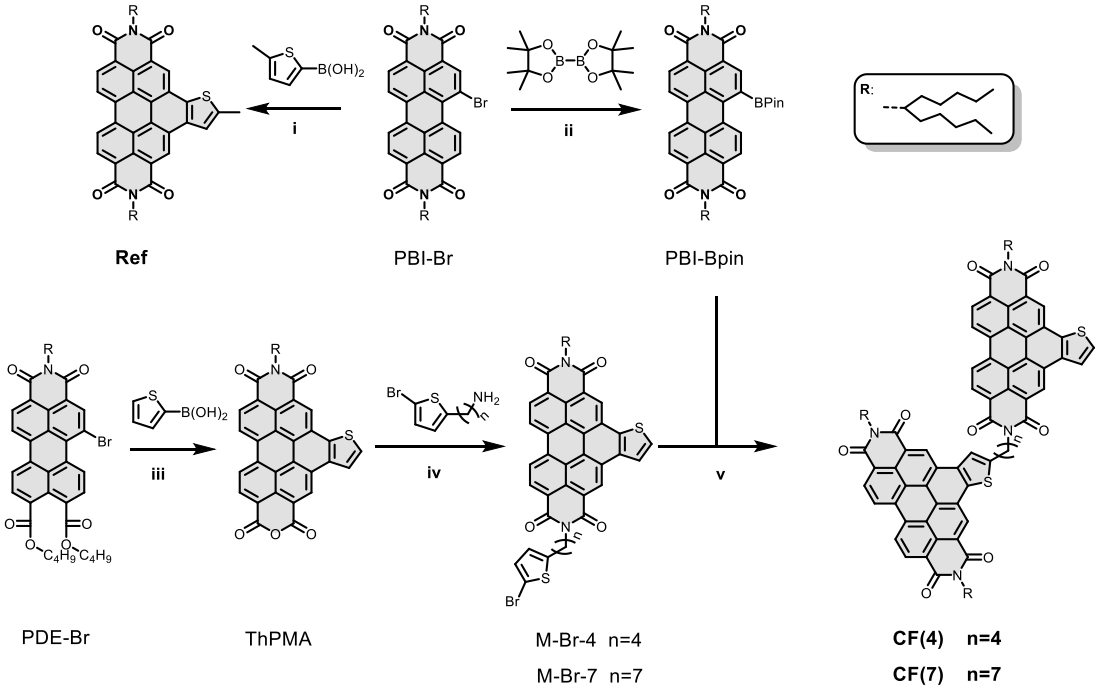

Scheme S1. Synthetic route to the target compounds. Reaction conditions: (i) 2-methyl-5-thiopheneboronic acid, K_2CO_3(aq), $Pd(PPh_3)_4$, TOL, 95 °C, 8 h; $CHCl_3$, I_2, hv, r.t., 2 h; (ii) $(Bpin)_2$, KH_2PO_4, $PdCl_2$(dppf), TOL, 95 °C, 24 h; (iii) 2-Thiophene boronic acid, K_2CO_3(aq), $Pd(PPh_3)_4$, TOL, 95 °C, 8 h; $CHCl_3$, I_2, hv, r.t., 2 h; (iv) Imidazole, $Zn(OAc)_2$, 140 °C, 8 h; (v) $Pd_2(dba)_3$, S-Phos, K_2CO_3(aq), TOL, 95 °C, 12 h; $CHCl_3$, I_2, hv, r.t., 2 h.

The synthesis of the linker 5-(aminoalkyl)-2-bromothiophene was carried out according to reported procedures with minor modifications.[1,2] Varying the alkyl chain length showed no significant influence on reaction efficiency under standard conditions. The starting materials PBI-Br and PDE-

Br were synthesized following previously reported methods.[3,4] During bromination of PDE in liquid bromine, substitution preferentially occurred at the imide side rather than at the bay position of the ester group, attributable to the asymmetric electron distribution of the perylene core, consistent with literature reports. Subsequent Suzuki coupling and photocyclization afforded ThPDE, in which the sulfur atom is oriented toward the imide side. Detailed synthetic procedures are described below.

Synthesis of Ref:

A 50 mL Schlenk flask was charged with PBI-Br (100 mg, 0.12 mmol), 2-methyl-5-thiopheneboronic acid (43 mg, 0.24 mmol, 2.0 equiv), and $Pd(PPh_3)_4$ (12 mg, 10 mol%). TOL (12 mL) and an aqueous solution of K_2CO_3 (1 N, 6 mL) were added by syringe. The reaction mixture was heated to 95 °C under a nitrogen atmosphere with stirring for 12 h. After cooling to room temperature, the reaction mixture was extracted with ethyl acetate (3 × 20 mL). The combined organic layers were dried over anhydrous $MgSO_4$, filtered, and concentrated under reduced pressure. The crude product was purified by silica gel column chromatography using dichloromethane/petroleum ether (2:1, v/v) as the eluent. All synthetic operation was conducted in the dark.

The resulting intermediate was dissolved in dichloromethane (20 mL), followed by the addition of iodine. The solution was irradiated with a 365 nm mercury lamp at room temperature for 2 h. After completion (monitored by TLC), the solvent was removed under reduced pressure, and the residue was purified by column chromatography (dichloromethane/petroleum ether, 2:1, v/v) to afford Ref as an orange-yellow solid (78 mg, 76% overall yield over two steps). MALDI-TOF(m/z): calcd. for $C_{51}H_{56}N_2O_4S_1$ 792.40; found, 790.3400.; ^{1}H NMR (400 MHz, $CDCl_3$) δ 9.33 (s, 1H), 9.11 (s, 1H), 8.93 (d, J = 8.3 Hz, 4H), 7.97 (s, 1H), 5.41–5.26 (m, 2H), 3.02–2.94 (m, 3H), 2.40 (d, J = 7.5 Hz, 4H), 2.03 (s, 4H), 1.52–1.30 (m, 25H), 0.93–0.80 (m, 12H).

Synthesis of CF(4):

A 25 mL Schlenk flask was charged with M-Br-4 (100 mg, 0.12 mmol), PBI-Bpin (98 mg, 0.12 mmol, 1.0 equiv), $Pd_2(dba)_3$ (11 mg, 10 mol%), and S-Phos (6.6 mg). TOL (5 mL) and aqueous K_2CO_3 (1 N, 0.5 mL) were added by syringe. The reaction mixture was heated to 95 °C under nitrogen with stirring for 12 h. After cooling, the crude mixture was extracted with dichloromethane. The combined organic layers were dried over anhydrous $MgSO_4$, filtered, and concentrated under reduced pressure. The residue was purified by silica gel chromatography using dichloromethane as the eluent. All synthetic operation was conducted in the dark.

The intermediate was dissolved in $CHCl_3$ (50 mL), followed by the addition of iodine. The solution was irradiated with a 365 nm mercury lamp at room temperature for 2 h. After completion, the solvent was removed, and the crude product was purified by column chromatography ($CHCl_3$) to afford **CF(4)** as an orange-red solid (80 mg, 46% overall yield over two steps). MALDI-TOF(m/z): calcd. for $C_{93}H_{92}N_4O_8S_2$ 1456.60; found, 1455.89.; ^{1}H NMR (600 MHz, $C_2D_2Cl_4$, 333 K) δ 8.99 (s, 1H), 8.90 (s, 1H), 8.61 (d, J = 8.0 Hz, 3H), 8.52 (d, J = 7.9 Hz, 1H), 8.45 – 8.31 (m, 5H), 8.26 (d, J = 8.0 Hz, 1H), 7.79 (s, 1H), 7.65 (d, J = 5.0 Hz, 1H), 7.59 (s, 1H), 5.47 – 5.37 (m, 1H), 5.25 (q, J = 7.3 Hz, 2H), 4.33 (s, 2H), 3.23 – 3.13 (m, 2H), 2.54 – 2.46 (m, 2H), 2.33 (s, 8H), 2.12 (s, 6H), 1.56 – 1.43 (m, 36H), 0.99 (m, J = 24.2, 12.1, 7.1 Hz, 18H).

Synthesis of CF(7):

A 25 mL Schlenk flask was charged with M-Br-7 (100 mg, 0.115 mmol), PBI-Bpin (98 mg, 0.115 mmol, 1.0 equiv), $Pd_2(dba)_3$ (11 mg, 10 mol%), and S-Phos (6.6 mg). TOL (5 mL) and aqueous K_2CO_3 (1 N, 0.5 mL) were added by syringe. The reaction mixture was heated to 95 °C under nitrogen with stirring for 12 h. After cooling, the crude mixture was extracted with dichloromethane. The combined organic layers were dried over anhydrous $MgSO_4$, filtered, and concentrated under reduced pressure. The residue was purified by silica gel chromatography using dichloromethane as the eluent. All synthetic operation was conducted in the dark.

The intermediate was dissolved in $CHCl_3$ (50 mL), followed by the addition of iodine. The solution was irradiated with a 365 nm mercury lamp at room temperature for 2 h. After completion, the solvent was removed, and the crude product was purified by column chromatography ($CHCl_3$) to afford **CF(7)** as a red solid (89 mg, 52% overall yield over two steps). MALDI-TOF(m/z): calcd. for $C_{96}H_{98}N_4O_8S_2$ 1498.70; found, 1497.37.; ^{1}H NMR (600 MHz, $C_2D_2Cl_4$, 333 K) δ 8.29 – 7.61 (m, 6H), 7.60 – 7.17 (m, 6H), 6.94 (s, 3H), 5.12 (d, J = 67.9 Hz, 3H), 4.03 (s, 2H), 3.08 (s, 2H), 2.36 – 2.10 (m, 8H), 2.01 (d, J = 35.1 Hz, 6H), 1.86 (s, 2H), 1.64 (d, J = 17.5 Hz, 6H), 1.48 (s, 36H), 1.04 (t, J = 29.2 Hz, 18H).

Synthesis of PBI-Bpin:

A 100 mL Schlenk flask was charged with PBI-Br (1.50 g, 1.93 mmol), $(Bpin)_2$ (1.47 g, 5.79 mmol), KH_2PO_4 (4.26 g, 19.3 mmol), and $PdCl_2$(dppf) (140 mg, 10 mol%) in 60 mL TOL solvent. After six nitrogen purge cycles, the mixture was heated to 140 °C with vigorous stirring for 24 h. Upon cooling, the reaction mixture was extracted with ethyl acetate (3 × 30 mL) and water (50 mL). The combined organic layers were dried over anhydrous $MgSO_4$, concentrated, and purified by flash column chromatography (dichloromethane/petroleum ether) to afford PBI-Bpin as a red solid (1.28 g, 78%). It should be noted that due to the instability of pinacol ester, our sample failed to yield a pure NMR spectrum after column chromatography, particularly in the high-field region where certain hydrogen signals attributed to the pinacol methyl group remained problematic. The problematic NMR spectrum is presented below. ^{1}H NMR (400 MHz, $CDCl_3$) δ 8.81 (d, *J* = 11.5 Hz, 1H), 8.73 – 8.56 (m, 5H), 8.35 (d, *J* = 7.9 Hz, 1H), 5.27 – 5.11 (m, 2H), 2.26 (dt, *J* = 14.5, 9.7 Hz, 4H), 1.98 – 1.75 (m, 4H), 1.50 (s, 8H), 1.43 – 1.12 (m, 24H), 0.84 (dt, *J* = 7.3, 3.5 Hz, 12H).

Synthesis of ThPDE：

A 50 mL Schlenk flask was charged with PDE-Br (0.50 g, 0.66 mmol), thiophene-2-boronic acid (0.42 g, 3.30 mmol, 5.0 equiv), and $Pd(PPh_3)_4$ (40 mg, 5 mol%). TOL (12 mL) and aqueous K_2CO_3 (1 M, 6 mL) were added, and the mixture was heated at 95 °C under nitrogen for 12 h. After cooling, the crude product was extracted with ethyl acetate (3 × 20 mL), dried over $MgSO_4$, and purified by silica gel chromatography (dichloromethane/petroleum ether, 2:1). All synthetic operation was conducted in the dark.

The intermediate was dissolved in 100 mL dichloromethane, followed by the addition of iodine. The solution was irradiated with a 365 nm Hg lamp at room temperature for 2 h. Purification by column chromatography (dichloromethane) afforded ThPDE as an orange-yellow solid (0.30 g, 60% overall yield).

Synthesis of ThPMA：

A 100 mL Schlenk flask was charged with ThPDE (0.30 g, 0.40 mmol) and p-TsOH·H_2O (0.41 g, 2.40 mmol, 6.0 equiv) dissolved in 40 mL TOL. The mixture was refluxed at 110 °C under reflux for 12 h under N_2 atmosphere. After cooling to room temperature, the precipitate was collected via

vacuum filtration, sequentially washed with deionized water (3 × 10 mL) and methanol (3 × 10 mL), and dried under vacuum to afford ThPMA as an orange-red solid (0.24 g, 96% yield). ^{1}H NMR (400 MHz, $CDCl_3$) δ 9.41 (m, 1H), 9.39 (m, 1H), 9.06 (dd, J = 13.7, 8.3 Hz, 2H), 8.95 (s, 1H), 8.85 (d, J = 8.2 Hz, 1H), 8.25 (d, J = 5.4 Hz, 1H), 8.03 (d, J = 5.4 Hz, 1H), 2.40 – 2.25 (m, 2H), 1.95 (s, 2H), 1.19 (s, 12H), 0.81 (d, J = 2.3 Hz, 6H).

Synthesis of M-Br-4:

A 100 mL three-neck flask was charged with ThPMA (0.24 g, 0.38 mmol), 5-(n-aminobutyl)-2-bromothiophene (0.13 g, 0.57 mmol, 1.5 equiv), zinc acetate (0.20 g, 1.09 mmol, 2.9 equiv), and imidazole (3.0 g, 44.1 mmol, 116 equiv) under N_2 atmosphere. The mixture was heated to 140 °C and stirred for 24 h. After cooling, the reaction was quenched with HCl (1 N, 20 mL), inducing immediate precipitation. The crude product was stirred for 30 min, isolated via vacuum filtration, and sequentially washed with deionized water (3 × 15 mL), methanol (3 × 15 mL), and dichloromethane (2 × 10 mL). Final purification by silica gel chromatography in dichloromethane yielded M-Br-4 as an orange-red solid (0.30 g, 90%).^{1}H NMR (400 MHz, $CDCl_3$) δ 8.35 (s, 1H), 8.29 (s, 1H), 7.88 (d, J = 8.1 Hz, 1H), 7.80 (d, J = 7.9 Hz, 1H), 7.72 (s, 1H), 7.65 (s, 1H), 7.47 (d, J = 5.1 Hz, 1H), 7.15 (d, J = 5.1 Hz, 1H), 6.92 (d, J = 3.5 Hz, 1H), 6.68 (d, J = 3.6 Hz, 1H), 5.23 (m, 1H), 3.99 (t, J = 6.7 Hz, 2H), 2.94 (t, J = 7.4 Hz, 2H), 2.43 – 2.25 (m, 2H), 2.07 (m, 2H), 1.85 – 1.77 (m, 4H), 1.53 – 1.41 (m, 12H), 0.99 (t, J = 6.9 Hz, 6H).

Synthesis of M-Br-7:

A 100 mL three-neck flask was charged with ThPMA (0.24 g, 0.38 mmol), 5-(n-aminoheptyl)-2-bromothiophene (0.15 g, 0.57 mmol, 1.5 equiv), zinc acetate (0.20 g, 1.09 mmol, 2.9 equiv), and imidazole (3.0 g, 44.1 mmol, 116 equiv) under N_2 atmosphere. The mixture was heated to 140 °C and stirred for 24 h. After cooling, the reaction was quenched with HCl (1 N, 20 mL), inducing immediate precipitation. The crude product was stirred for 30 min, isolated via vacuum filtration, and sequentially washed with deionized water (3 × 15 mL), methanol (3 × 15 mL), and dichloromethane (2 × 10 mL). Final purification by silica gel chromatography in dichloromethane yielded M-Br-7 as an orange-red solid (0.33 g, 94%). ^{1}H NMR (400 MHz, $CDCl_3$) δ 8.31 (d, J = 3.5 Hz, 1H), 8.28 (s, 1H), 7.85 (d, J = 8.1 Hz, 1H), 7.82 – 7.75 (m, 1H), 7.67 (s, 1H), 7.63 (d, J = 8.1 Hz, 1H), 7.44 (d, J = 5.1 Hz, 1H), 7.10 (d, J = 5.1 Hz, 1H), 6.89 (d, J = 3.5 Hz, 1H), 6.62 (d, J = 3.6 Hz, 1H), 5.23 (ddd, J = 14.7, 8.5, 6.1 Hz, 1H), 4.07 – 3.87 (m, 2H), 2.83 (dt, J = 14.8, 7.7 Hz, 2H), 2.34 (ddt, J = 17.7, 13.9, 6.3 Hz, 2H), 2.08 (qd, J = 12.1, 9.1, 4.0 Hz, 2H), 1.81 – 1.70 (m, 4H), 1.58 – 1.44 (m, 16H), 1.00 (t, J = 6.9 Hz, 6H).

3. DFT Calculation

Density Functional Theory (DFT) calculations were performed in Gaussian09. The ground-state geometries of different conformations were fully optimized using the *ω*B97XD/def2SVP level of theory. The frontier molecular orbitals were calculated at the optimized ground-state geometries using the same level of theory. The reported S_1 and T_1 values in this work were obtained as vertical excitation energies at the S_0-optimized geometries using TDDFT in Gaussian.

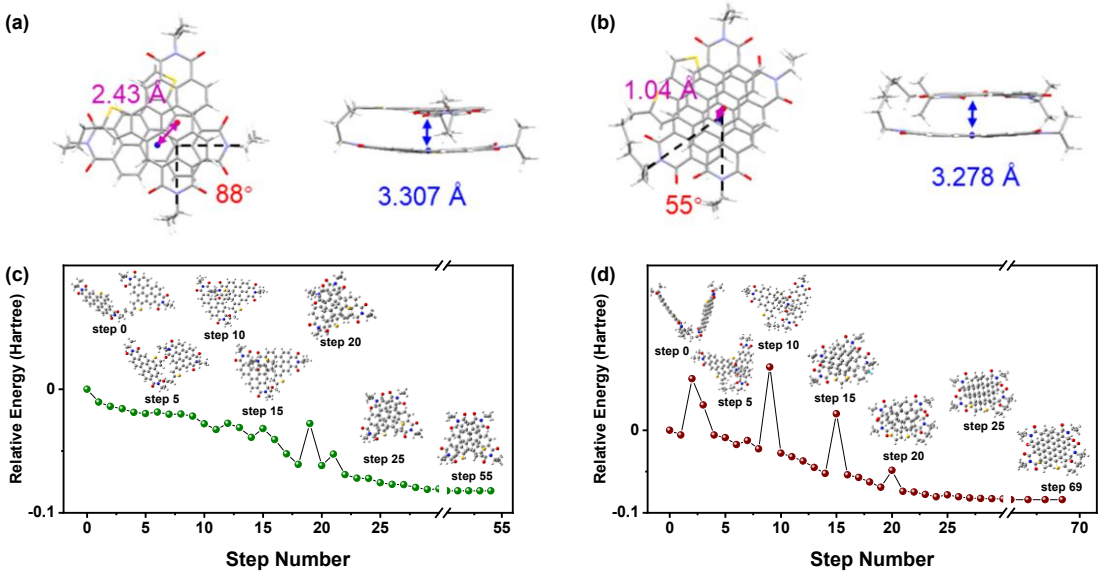

Figure S1. DFT-optimized structures of (a) **CF(4)** and (b) **CF(7)** calculated at the *ω*B97XD/def2SVP level. The side view (left) and the top view (right) are shown. The slip distance is shown in purple, the rotational angle between the monomer in red, and the π-π stacking distance in blue. Evolution of the relative energy during the geometry optimization of (c) **CF(4)** and (d) **CF(7)**, respectively, starting from unfolded initial structures (step 0), together with representative geometries at selected optimization steps. The optimization shows spontaneous structural relaxation from unfolded conformations toward folded structures.

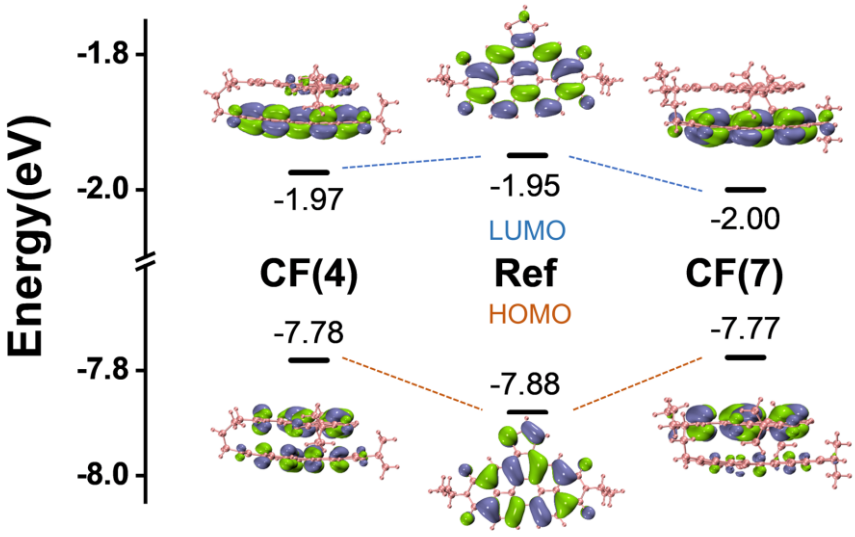

Figure S2. Molecular orbital (MO) energy levels and corresponding orbital isosurfaces of Ref, **CF(4)**, and **CF(7)** calculated at the *ω*B97XD/def2SVP level. The highest occupied molecular orbital (HOMO) and lowest unoccupied molecular orbital (LUMO) energies are indicated for each system. Dashed lines illustrate the relative splitting of the frontier orbital energy levels from Ref to **CF(4)** and **CF(7)**. (isovalue = 0.03)

Table S1. Energy level of singlet and triplet state of Ref and PBI.

Molecule	Ref	PBI
S_1 /eV	2.961	2.744
T_1 /eV	1.497	1.108
$\Delta(2T_1\text{-}S_1)$ /eV	0.033	-0.528

The exciton coupling calculation is based on the optimized crossfoldamers structure and takes both short-range CT coupling and long-range Coulomb coupling into consideration. The Coulombic coupling is calculated by the point atomic charges method as expressed,[5] in the following Eq. S1:

$$J_{coul} = \frac{1}{4\pi\varepsilon_0}\sum_i\sum_j \frac{q_i^{(1)}q_j^{(2)}}{\left|r_i^{(1)}-r_j^{(2)}\right|} \qquad \text{(Eq. S1)}$$

$\boldsymbol{\varepsilon_0}$ is the dielectric constant of the medium, $\boldsymbol{q_i}$ presents the transition charge on atom $\boldsymbol{i}$ of chromophore, $\boldsymbol{r_i}$ corresponds to the position vector of the respective transition charge. Superscripts (1) and (2) correspond respectively to monomer fragments (1) and (2) within the dimer. All the J_{Coul} calculated in this article were based on Eq. S1.

The short-range CT coupling arises via a virtual charge-transfer-mediated superexchange mechanism, governed by the frontier orbital overlap between the two chromophores. J_{CT} is calculated as:

$$J_{CT} = \frac{-2t_e t_h}{E_{CT}-E_{S1}} \qquad \text{(Eq. S2)}$$

where t_e and t_h denote the electron-transfer and hole-transfer integrals, respectively. The values for CT integrals t_e and t_h of dimers were calculated using the polarization-including energy splitting in the dimer model.[6,7] The energy difference $E_{CT\text{-}S1}$ represents the gap between the CT state and the lowest singlet excited state (S_1) and is set to 1500 cm^{-1} based on similar systems in the literature.[8] All the J_{CT} calculated in this article was based on Eq. S2. The total exciton coupling is the sum of the Coulombic coupling and CT coupling.

Table S2. Exciton coupling of **CF(4)** and **CF(7)** based on DFT-optimized Structure.

Molecule	χ (°)	t_e (cm^{-1})	t_h (cm^{-1})	J_{CT} (cm^{-1})	J_{Coul} (cm^{-1})	J_{Tot} (cm^{-1})
CF(4)	88	209.61	352.28	98.46	-137.99	-39.53
CF(7)	55	-555.19	436.80	323.34	396.39	719.73

4. Steady-State Absorption and Fluorescence Spectra

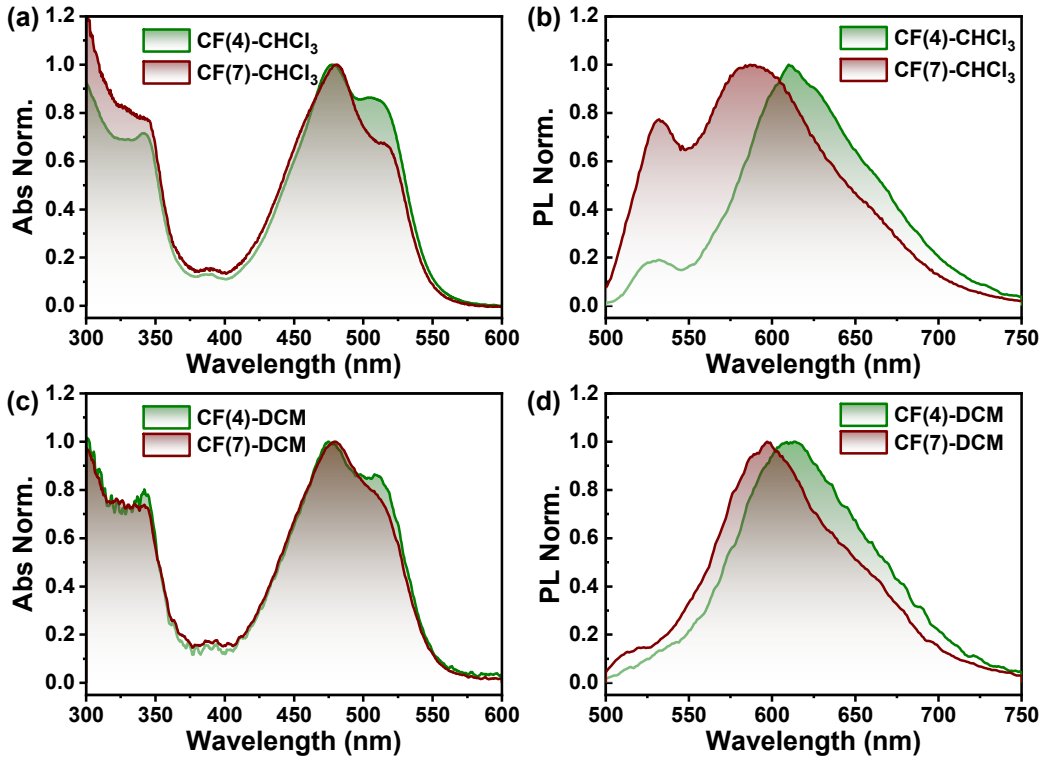

Figure S3. (a) Normalized UV-vis absorption and (b) normalized photoluminescence spectra of Ref, **CF(4)** and **CF(7)** in $CHCl_3$. (c) Normalized UV-vis absorption and (d) normalized photoluminescence spectra of Ref, **CF(4)** and **CF(7)** in DCM. ($c = 1.0 \times 10^{-6}$ M, $\lambda_{ex} = 450$ nm)

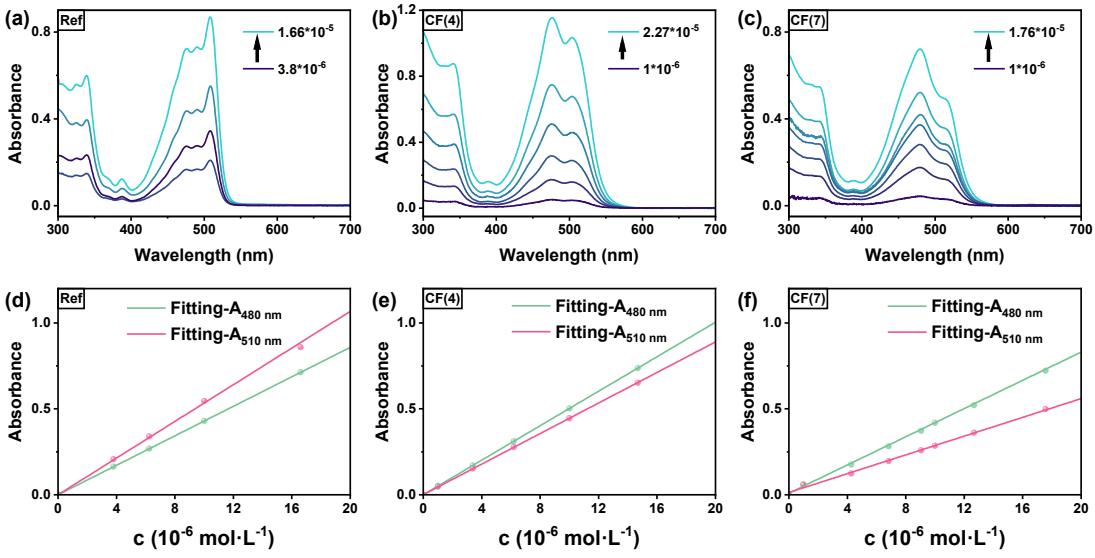

Figure S4. Concentration-dependent UV-vis absorption spectra of (a) Ref, (b) **CF(4)**, and (c) **CF(7)** recorded in TOL at different concentrations. The corresponding linear fitting of the absorbance at 480 nm and 510 nm versus concentration is shown for (d) Ref, (e) **CF(4)**, and (f) **CF(7)**.

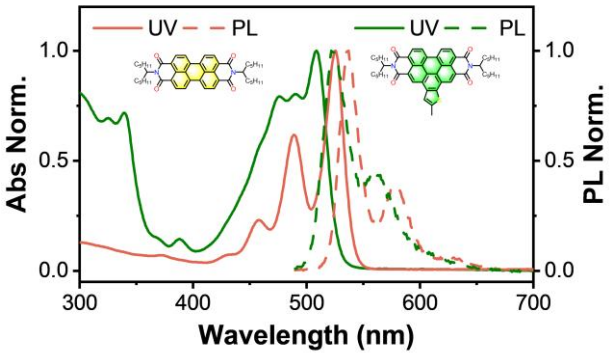

Figure S5. Comparison between PBI (orange) and Ref (green) in UV-vis absorption (solid line) and photoluminescence (dash line) spectra in TOL (c = 1.0 × 10^{-6} M).

Table S3. A_{0-1}/A_{0-0} of **CF(4)** and **CF(7)** in TOL and $CHCl_3$.

Molecule		**CF(4)**	**CF(7)**
A_{0-1}/A_{0-0}	TOL	1.111	1.493
	$CHCl_3$	1.159	1.494

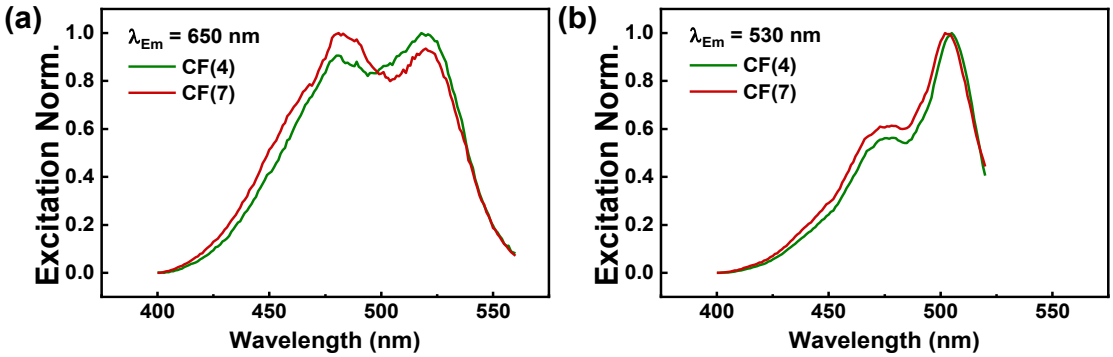

Figure S6. Excitation spectra for CF(4) and CF(7) in TOL solvent (a) at 650 nm emission and (b) at 530 nm emission.

5. PLQY

All the following quantum yields were determined with the relative method. The fluorescence standard, common perylene bisimide, is shown in Figure S5, whose quantum yield is near unity in all kinds of solvents.[9,10] In the fluorescence quantum yield measurement, the absorbance was maintained below 0.2 under all concentration ranges to minimize aggregation effects. An excitation wavelength of 480 nm was selected, and the corresponding emission spectra were recorded. The relative fluorescence quantum yield was determined by calculating the ratio of the integrated emission area to the absorbance at the excitation wavelength. This ratio was plotted for four different concentrations, and the slope was obtained via linear regression to derive the quantum yield. The relative PLQY of Ref, **CF(4)**, and **CF(7)** was shown in Table S4.

Considering that the emission spectrum contains both unfolded and folded conformations, we have decomposed the emission spectrum to obtain separate emission spectra corresponding to the unfolded and folded states, with their respective area ratios indicated in Figure S7. Although the unfolded conformation may exist within the system, its abundance is relatively low, with 81% and 90% of the emission originating from the folded state in TOL. Considering the proximity of several molecules' PLQY values, the emission intensity ratio is approximately proportional to the ratio of the unfolded/folded conformations. The approximate PLQYs of the crossfoldamers were calculated using $\Phi = \Phi_{ref} * a + \Phi_{fold} * (1-a)$, which a comes from $S_{unfolded}/S_{sum}$.

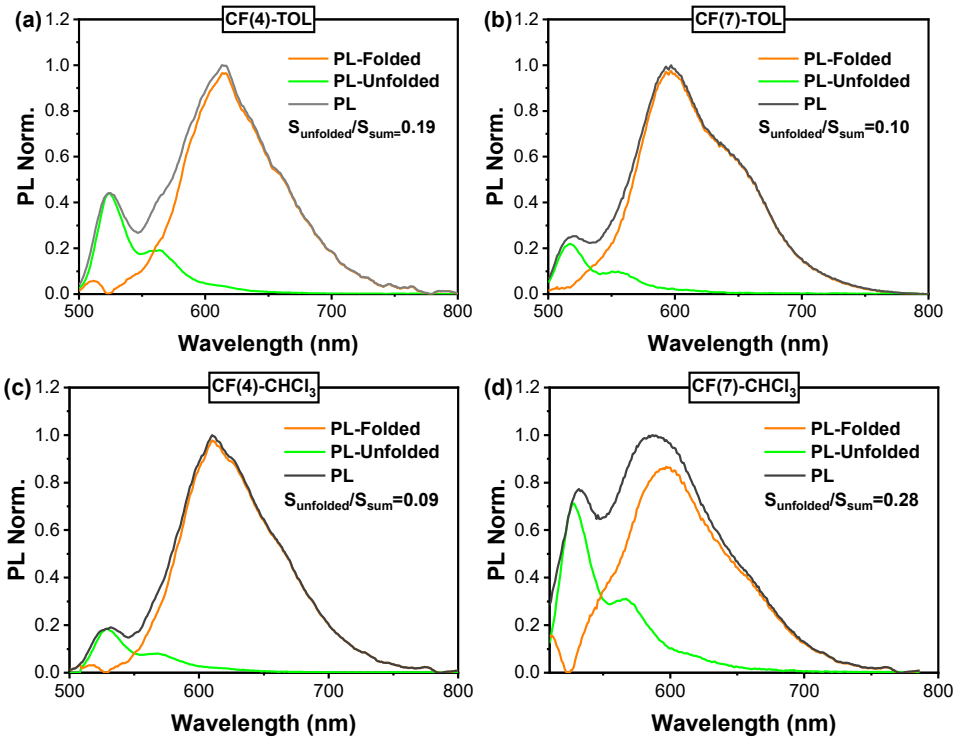

Figure S7. Deconvolution of the normalized PL spectra of crossfoldamers in different solvent. (a) CF(4) in TOL; (b) CF(7) in TOL; (c) CF(4) in $CHCl_3$; (d) CF(7) in $CHCl_3$. The PL (black) is expressed as the sum of the unfolded conformation (PL-Unfolded, orange) and the folded conformation (PL-Folded, green).

Table S4. PLQY of Ref, **CF(4)** and **CF(7)** in TOL and $CHCl_3$.

Molecule		Ref	**CF(4)**	**CF(7)**
Φ (%)	TOL	25.8	20.2	19.8
	$CHCl_3$	23.8	19.2	17.0
Φ_{fold} (%)	TOL	—	18.9	19.4
	CHCl3	—	18.7	14.3

6. Time-resolved Photoluminescence

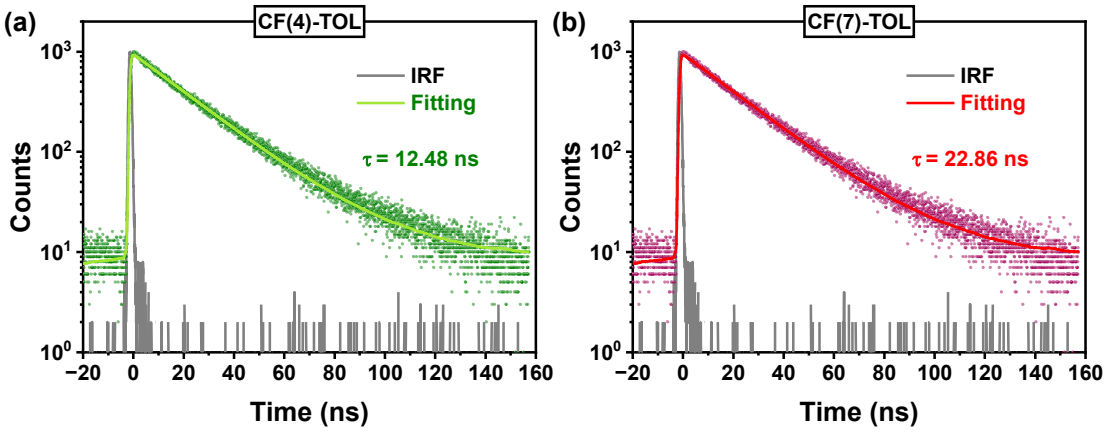

Figure S8. Time-resolved photoluminescence decay traces of (a) **CF(4)** and (b) **CF(7)** in TOL monitored at 650 nm. The measured instrument response function (IRF) is shown in grey, and the decay traces were fitted using IRF-convoluted monoexponential functions. The lifetimes are τ =12.48 ns for **CF(4)** and τ =22.86 ns for **CF(7)**.

Table S5. Radiative constant and nonradiative constant of Ref, **CF(4)** and **CF(7)** in TOL

Molecule	Ref	**CF(4)**	**CF(7)**
Φ (%)	25.8	18.9	19.1
τ (ns)	2.66	12.48	22.86
k_r (10^6 s^{-1})	0.097	0.015	0.0084
k_{nr} (10^6 s^{-1})	0.28	0.065	0.035

7. Ultrafast Transient Absorption

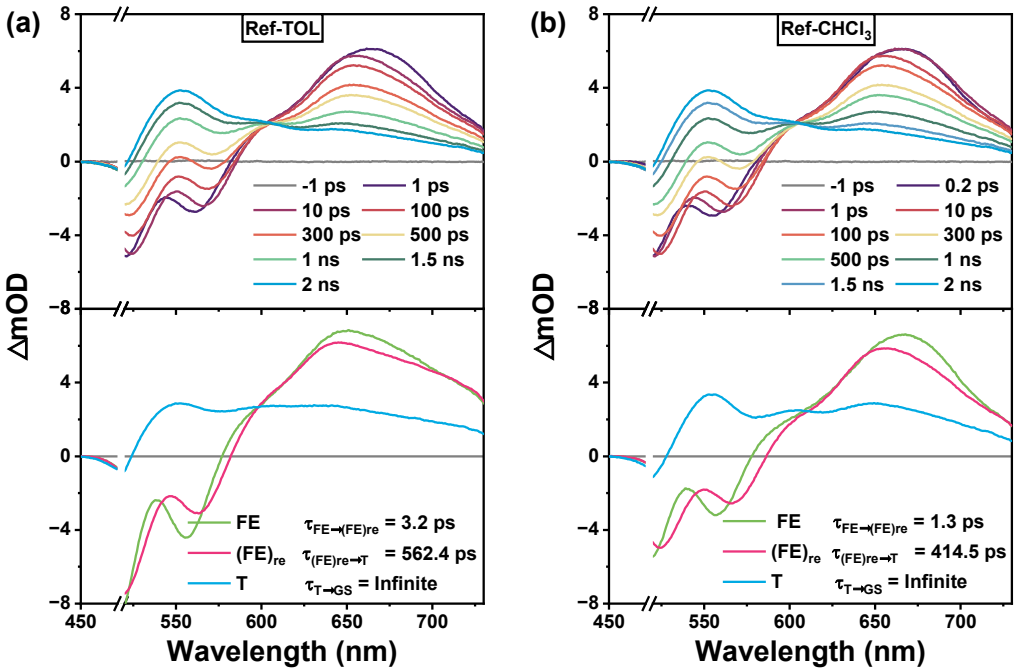

Figure S9. fs-TA spectra (top) and global analysis (bottom) of Ref in (a) TOL and (b) $CHCl_3$. Species identification and fitted lifetimes are also shown in the figure.

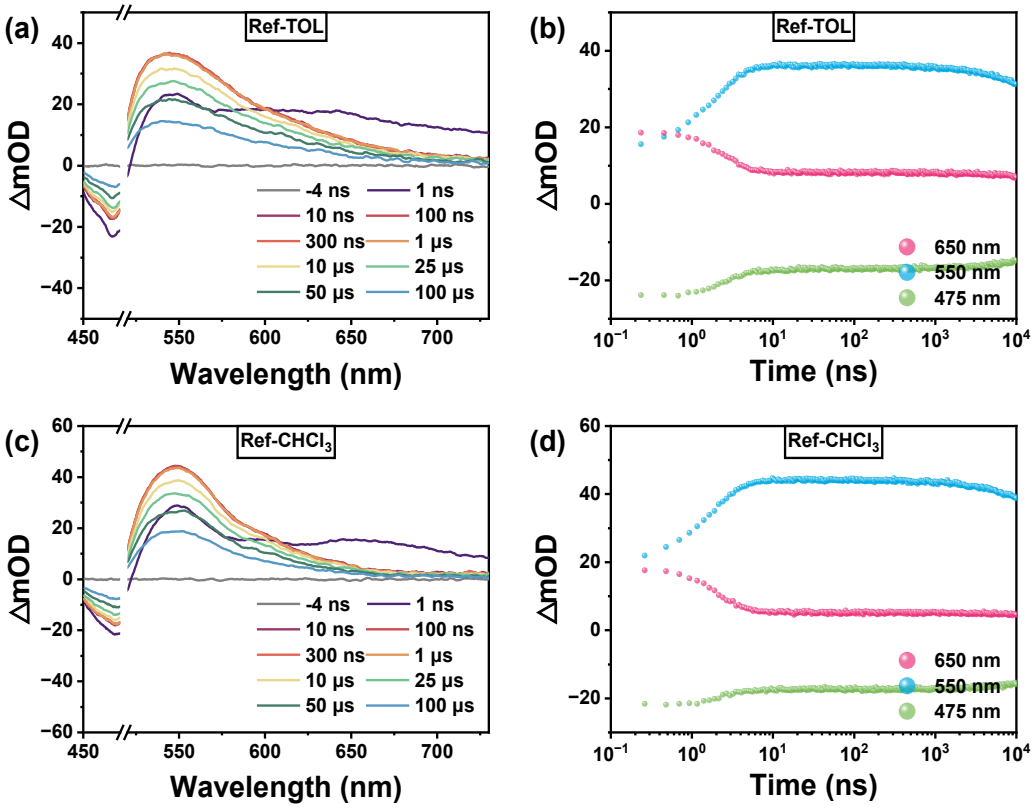

Figure S10. ns-TA spectra and kinetic traces at selected wavelengths of Ref: (a) ns-TA spectra and (b) kinetic traces in TOL, (c) ns-TA spectra and (d) kinetic traces in $CHCl_3$.

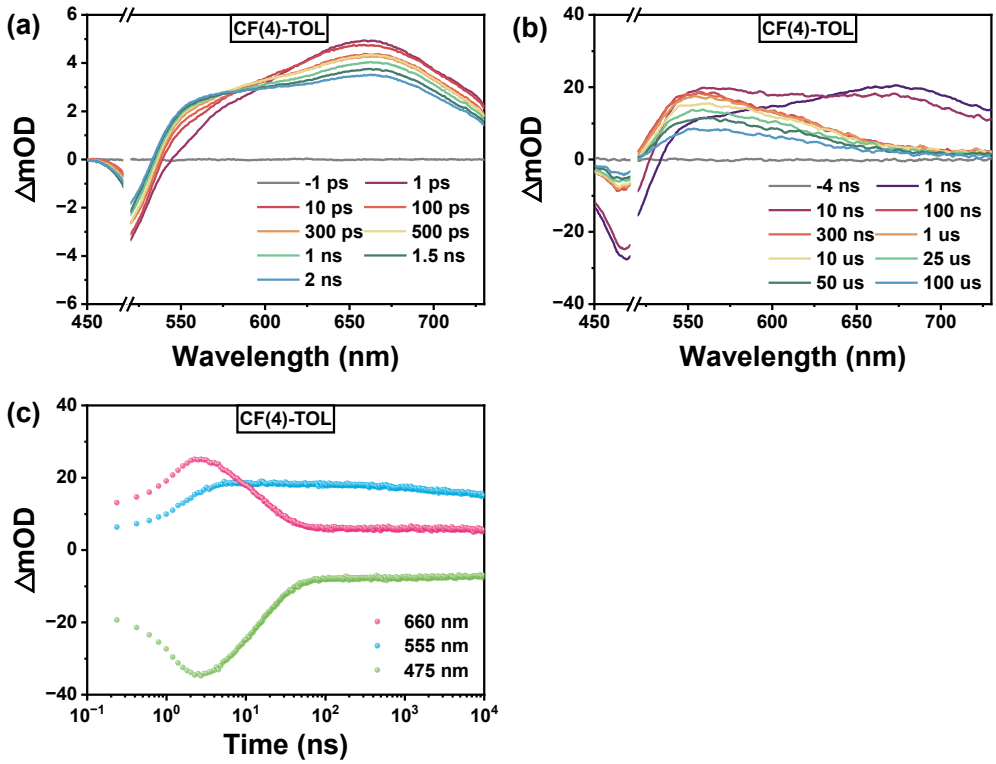

Figure S11. Ultrafast spectra data of **CF(4)** in TOL: (a) fs-TA spectra, (b) ns-TA spectra, and (c) kinetic traces at selected wavelengths derived from the ns-TA data.

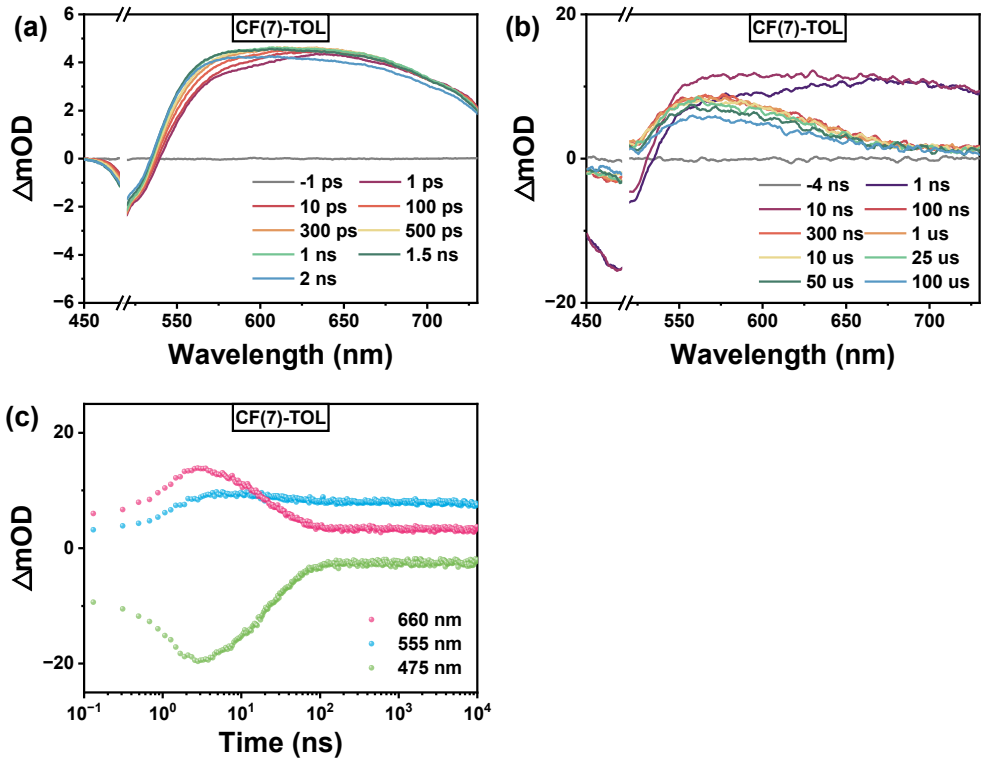

Figure S12. Ultrafast spectra data of **CF(7)** in TOL: (a) fs-TA spectra, (b) ns-TA spectra, and (c) kinetic traces at selected wavelengths derived from the ns-TA data.

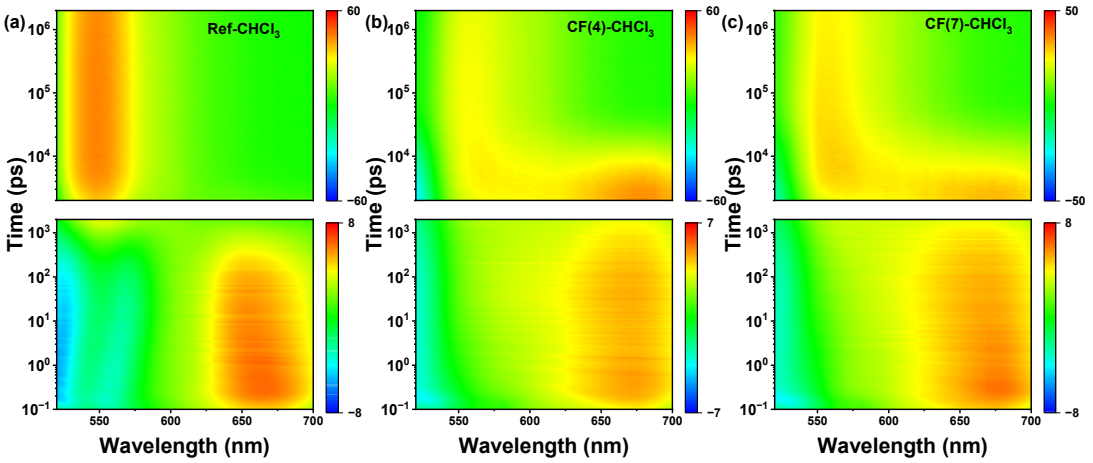

Figure S13. 2D heatmaps in $CHCl_3$ at fs and ns timescales for (a) Ref, (b) **CF(4)**, and (c) **CF(7)**.

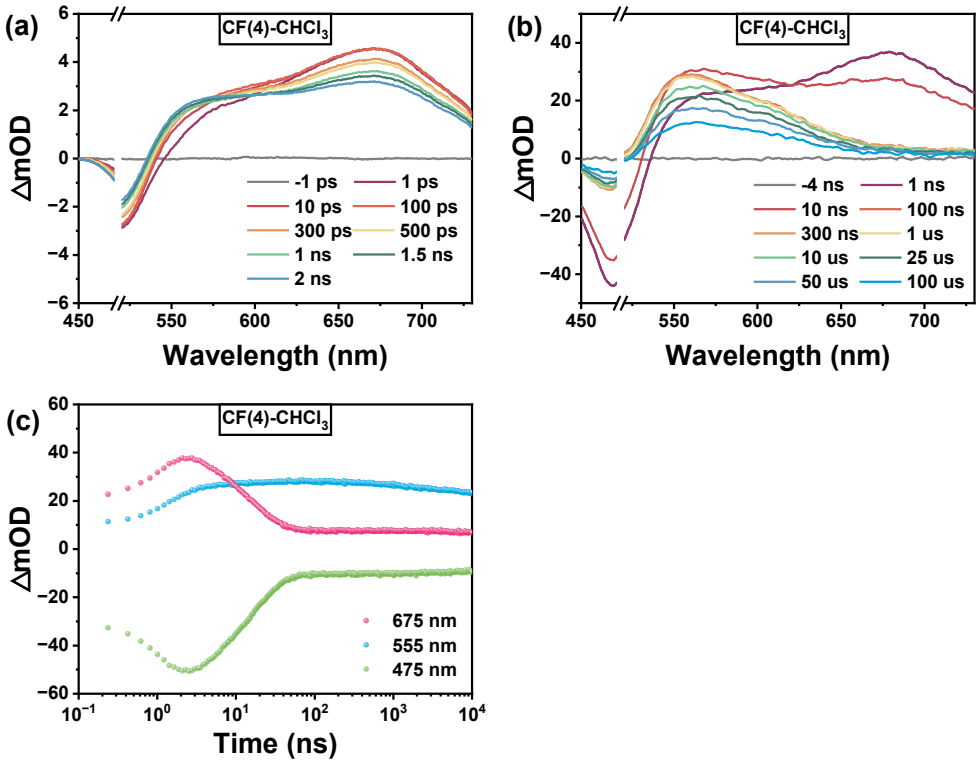

Figure S14. Ultrafast spectra data of **CF(4)** in $CHCl_3$: (a) fs-TA spectra, (b) ns-TA spectra, and (c) kinetic traces at selected wavelengths derived from ns-TA data.

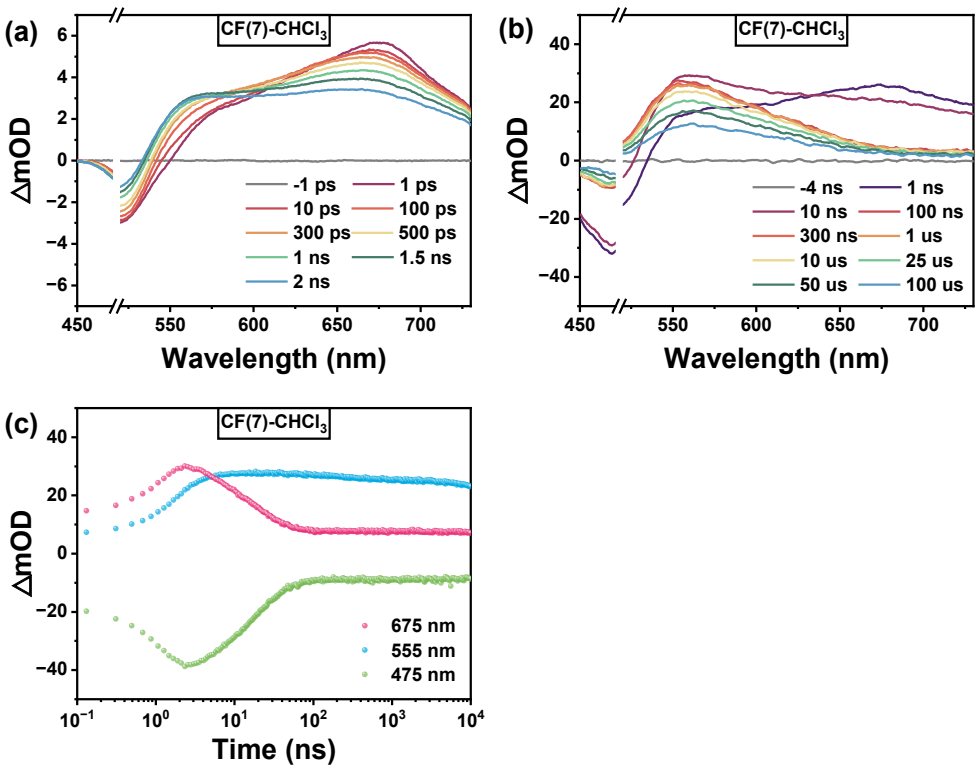

Figure S15. Ultrafast spectra data of **CF(7)** in $CHCl_3$: (a) fs-TA spectra, (b) ns-TA spectra, and (c) kinetic traces at selected wavelengths derived from the ns-TA data.

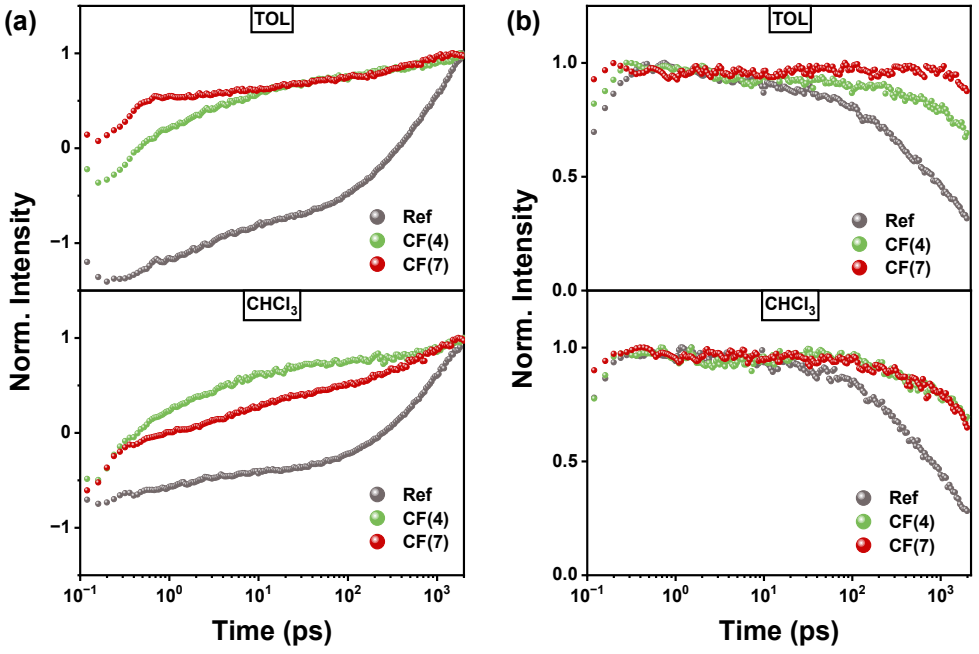

Figure S16. Comparison of fs-TA kinetics between **CF(4)** (green) and **CF(7)** (red) at (a) 555 nm and (b) 660 or 675 nm (Top: in TOL; Bottom: in $CHCl_3$). The kinetics of Ref (grey) is also given for comparison.

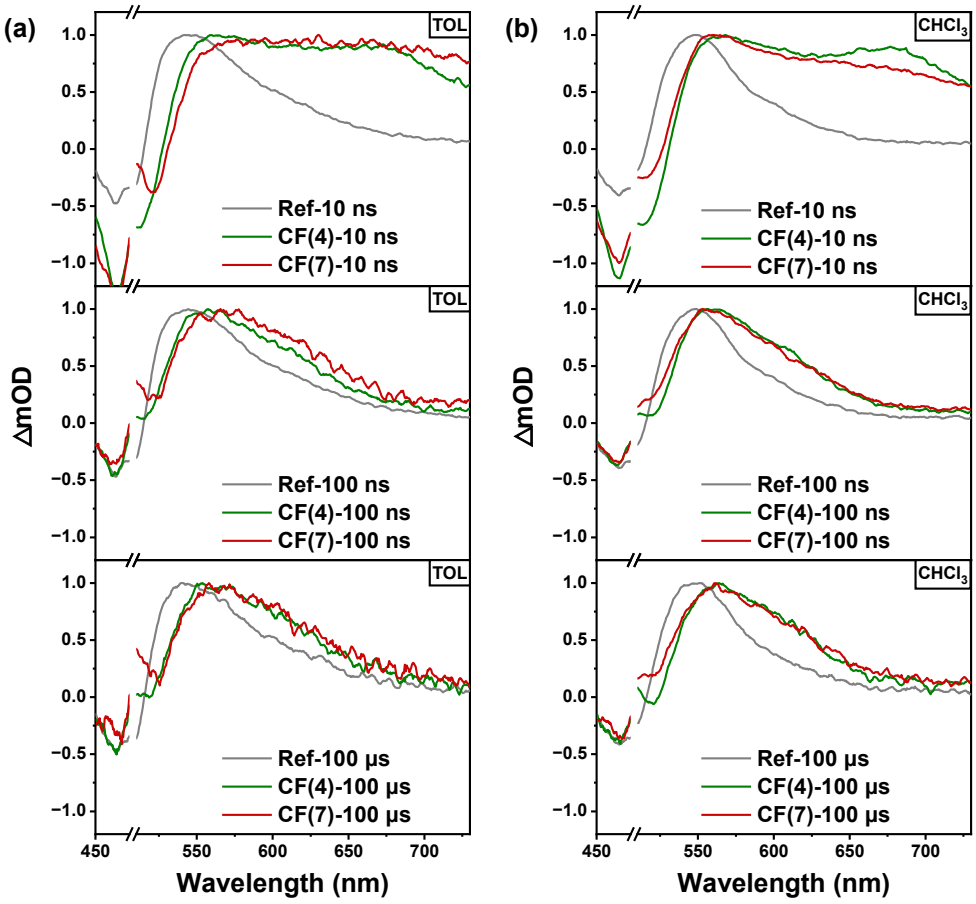

Figure S17. Comparison between the ME state for **CF(4)** (green), **CF(7)** (red) during different time scales in the ns-TA in (a) TOL and (b) $CHCl_3$. The triplet state of Ref (grey) is also given for comparison.

Table S6. Global fitting time constant in TA

Molecule	$FE^* \rightarrow FE_{relax}^*$	$FE^* \rightarrow T$	$T \rightarrow GS$
Ref (TOL)	3.2 ps	562.4 ps	64.2 µs
Ref($CHCl_3$)	1.3 ps	414.5 ps	68.7 µs
Molecule	$FE^* \rightarrow Ex^*$	$Ex^* \rightarrow ME^*$	$ME^* \rightarrow GS$
CF(4) (TOL)	0.4	27.1	76.5 µs
CF(7) (TOL)	1.1	113.9	214.9 µs
CF(4) ($CHCl_3$)	0.3	19.2	60.5 µs
CF(7) ($CHCl_3$)	0.7	84.8	71.9 µs

8. Triplet Yield Experiment

Singlet Oxygen Generation Experiment: The singlet oxygen quantum yield (Φ_Δ) was determined using the chemical probe method by monitoring the absorption bleaching of singlet oxygen probe 1,3-diphenylisobenzofuran (DPBF) at 414 nm to quantify the amount of $^1O_2$ generated. The singlet oxygen generation test requires triplet excitons with energy exceeding that of the singlet oxygen state (1270 nm, 0.98 eV) to enable efficient singlet oxygen production. In this system, the triplet exciton energy is 1.497 eV (Table S1), satisfying this energetic requirement. Experiments were conducted in TOL under irradiation at 500 nm (20 mW/cm^2). Diiodo-BODIPY was used as a reference compound, with a known singlet oxygen quantum yield in TOL of $\Phi_{\Delta,ref}$ = 0.87.[11] The sample to be tested was measured under identical conditions. The singlet oxygen quantum yield was calculated using Eq. S3:

$$\Phi_{\Delta,\mathrm{Sam}} = \Phi_{\Delta,\mathrm{Std}} \times \left(\frac{1-10^{1-A_{Std}}}{1-10^{1-A_{Sam}}}\right) \times \frac{m_{\mathrm{Sam}}}{m_{Std}} \qquad (\mathrm{Eq.\,S3})$$

In this equation, "sam" and "std" denote the sample and the reference standard, respectively; Φ_Δ is the singlet oxygen quantum yield; A is the absorbance at the excitation wavelength; m is the slope of the plot of the DPBF absorbance at 414 nm versus irradiation time. All measurements were performed in air-saturated TOL to ensure consistent oxygen concentration, and each experiment was repeated three times, with the results averaged to enhance accuracy. The data were listed in Table S4 below.

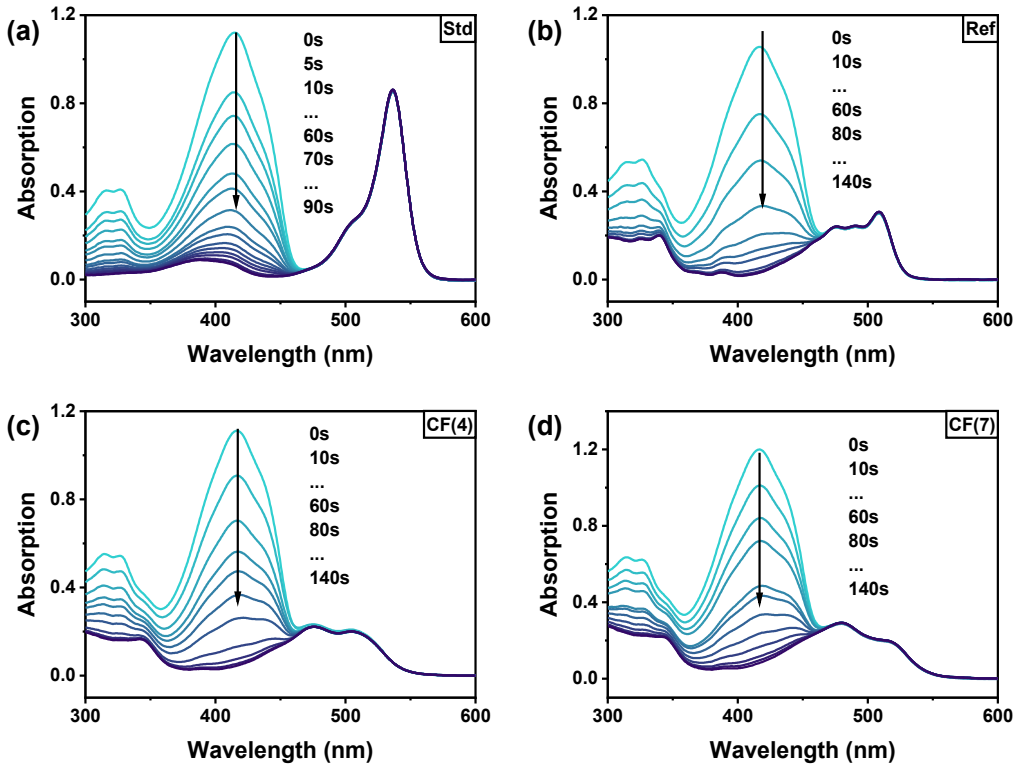

Figure S18. Singlet oxygen generation experiment for (a) Diiodo-BODIPY, (b) Ref, (c) **CF(4)** and (d) **CF(7)** in TOL.

Table S7. Singlet oxygen quantum yield of Ref, **CF(4)** and **CF(7)** in TOL

Molecule	BODIPY	Ref	**CF(4)**	**CF(7)**
A	0.18638	0.21251	0.19824	0.20851
m	-0.0488	-0.0389	-0.03387	-0.03959
Φ_Δ	0.87	0.625	0.575	0.645

Ground-state bleach recovery method: To estimate the triplet yield in our FE-ME-T system, a semi-quantitative method based on the ground-state bleach (GSB) recovery was employed.[12] The earliest GSB amplitude in the fsTA measurement was taken to represent the initial FE population (t_0 = 1 ps), while the residual GSB at the end of the fsTA time window was assigned mainly to ME (t_0 = 100 ps), giving an approximate ME/FE ratio. In the nsTA measurement, the earliest GSB amplitude was taken as the initial ME population, and the long-delay GSB plateau was assigned mainly to the triplet state, giving an approximate T/ME ratio. The fsTA and nsTA signal intensities were matched at the same delay time by the scaling factor *C*, typically 1 ns, using the GSB amplitude at the selected wavelength. The triplet yield was then estimated as:

$$\Phi_\Delta = \left(\frac{ME}{FE}\right) \times \left(\frac{T}{ME}\right) \times C \qquad (Eq.S4)$$

And the triplet yield can also be written directly as:

$$\Phi_\Delta = \left(\frac{A_{fs}(t_1)}{A_{fs}(t_0)}\right) \times \left(\frac{A_{ns}(t_2)}{A_{ns}(t_1)}\right) \times \left(\frac{A_{ns}(t_m)}{A_{fs}(t_m)}\right) \qquad (Eq.S5)$$

Here t_0 = 3 ps, t_2 = 100 ns and t_m = 1 ns. The amplitudes $A_{fs}(t_x)$ and $A_{ns}(t_x)$ are obtained from the GSB kinetic traces Figure S19. Using this qualitative or semi-quantitative ground-state bleach recovery method, the approximate triplet yields were determined to be 0.270 for Ref, 0.239 for CF(4), and 0.258 for CF(7). Accordingly, the triplet yield follows the trend of Ref > CF(7) > CF(4) (Table S8).

It should be emphasized that the GSB recovery analysis is only suitable for qualitative or semi-quantitative evaluation of the triplet yield, rather than an accurate determination of the absolute value. As summarized in Table S8, although the three systems may involve different triplet-generation pathways, their triplet yields are still within a similar range. Notably, the order of the estimated triplet yields, Ref > CF(7) > CF(4), is in good agreement with the trend observed for the singlet oxygen quantum yields.

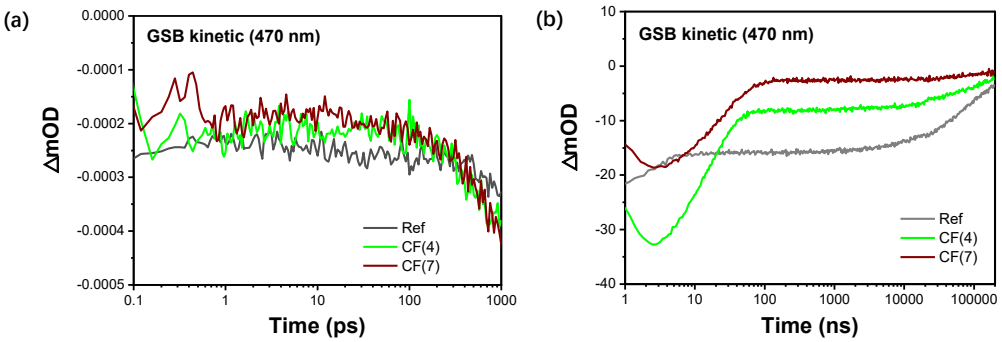

Figure S19. GSB kinetic at 470 nm for Ref (grey), CF(4) (green), CF(7) (red) in TOL solvent at (a) fsTA and (b) nsTA.

Table S8. Triplet yield of Ref, **CF(4)** and **CF(7)** in TOL based on GSB recovery method.

Molecule	**Ref**	**CF(4)**	**CF(7)**
fsTA (3ps)	$-2.15*10^{-4}$	$-2.04*10^{-4}$	$-2.02*10^{-4}$
fsTA (1000 ps)	$-3.26*10^{-4}$	$-3.80*10^{-4}$	$-4.25*10^{-4}$
nsTA (1 ns)	-15.35	-8.03	-2.74
nsTA（100ns）	-6.30	-3.58	-1.49
Φ_{Δ}(%)	27.0	23.9	25.8

9. NMR Spectra

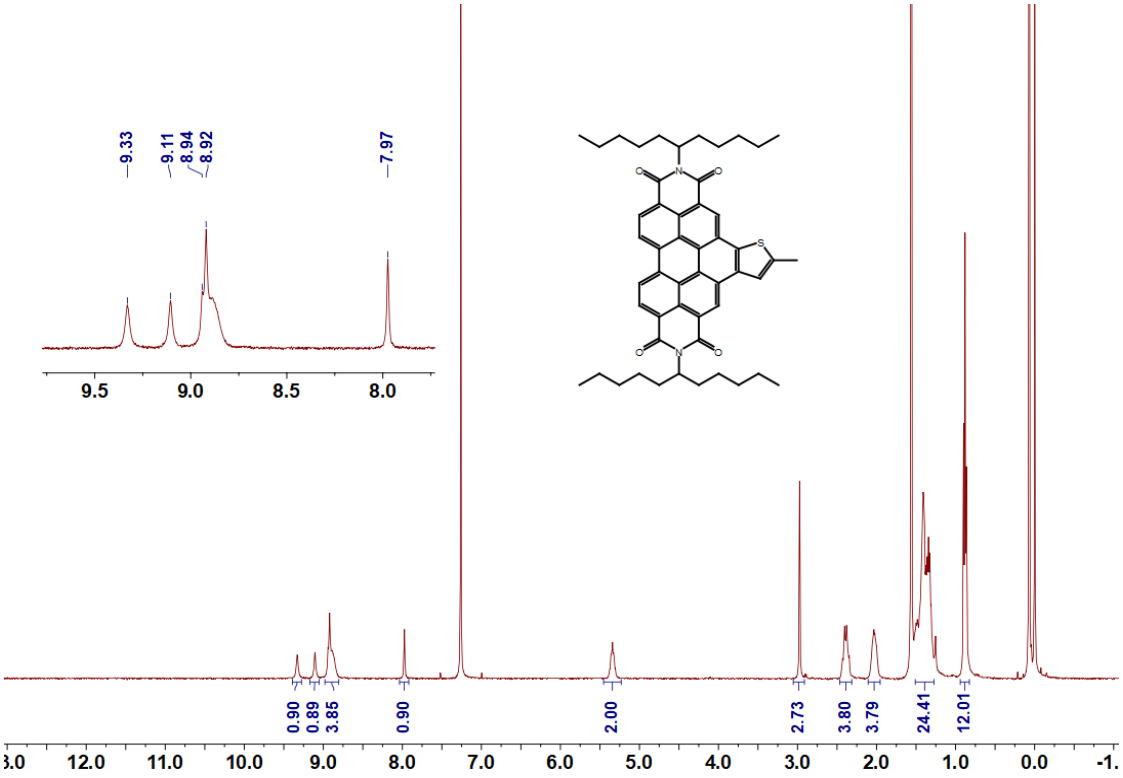

Figure S20. ^{1}H NMR spectrum of Ref (400 MHz, $CDCl_3$).

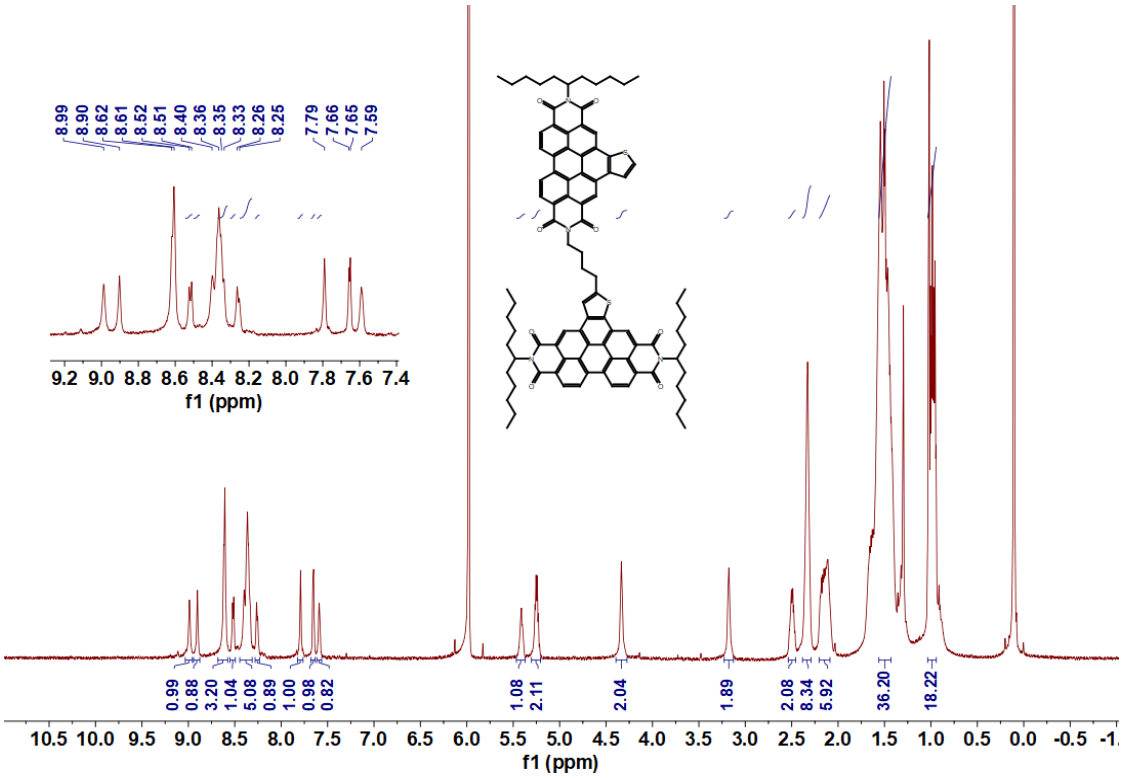

Figure S21. ^{1}H NMR spectrum of **CF(4)** (600 MHz, $C_2D_2Cl_4$, 333 K).

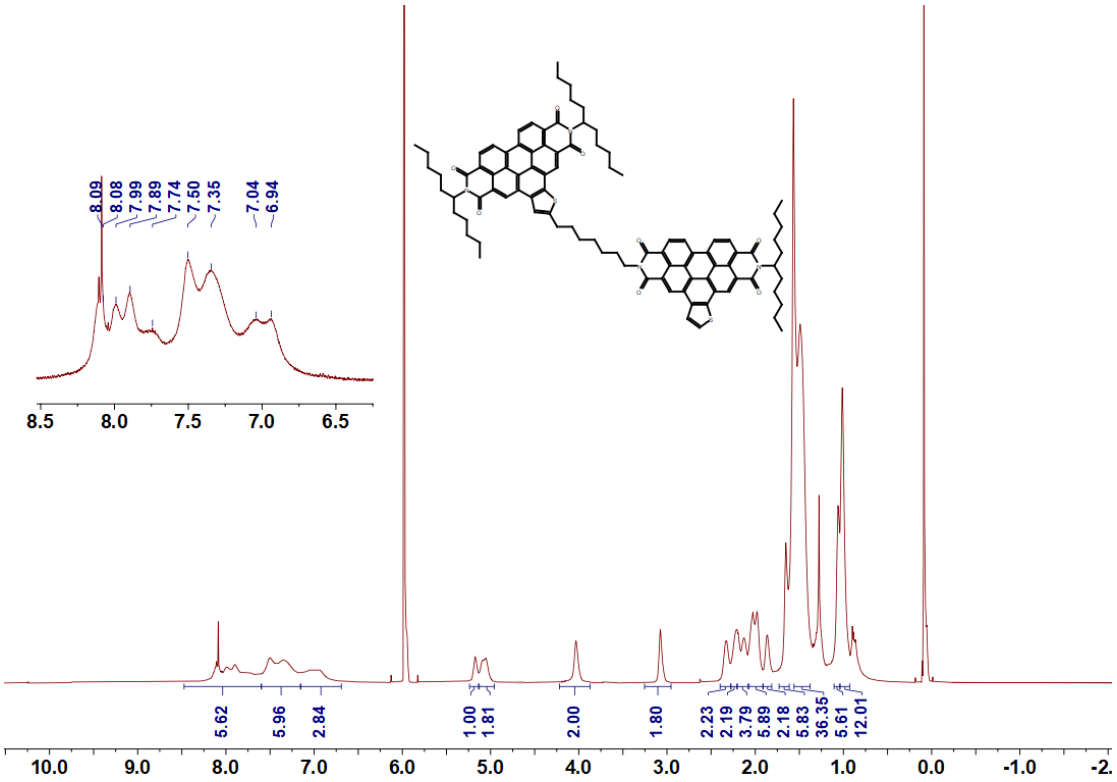

Figure S22. ^{1}H NMR spectrum of **CF(7)** (600 MHz, $C_2D_2Cl_4$, 333 K).

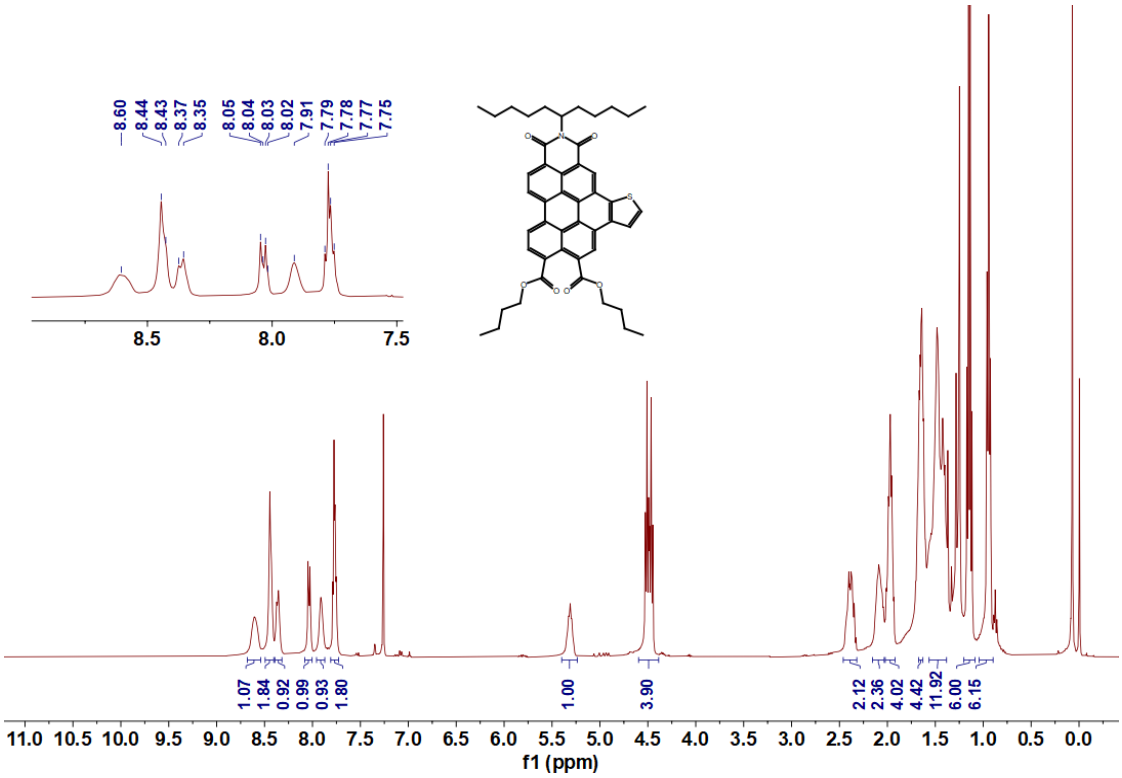

Figure S23. ^{1}H NMR spectrum of ThPDE (400 MHz, $CDCl_3$).

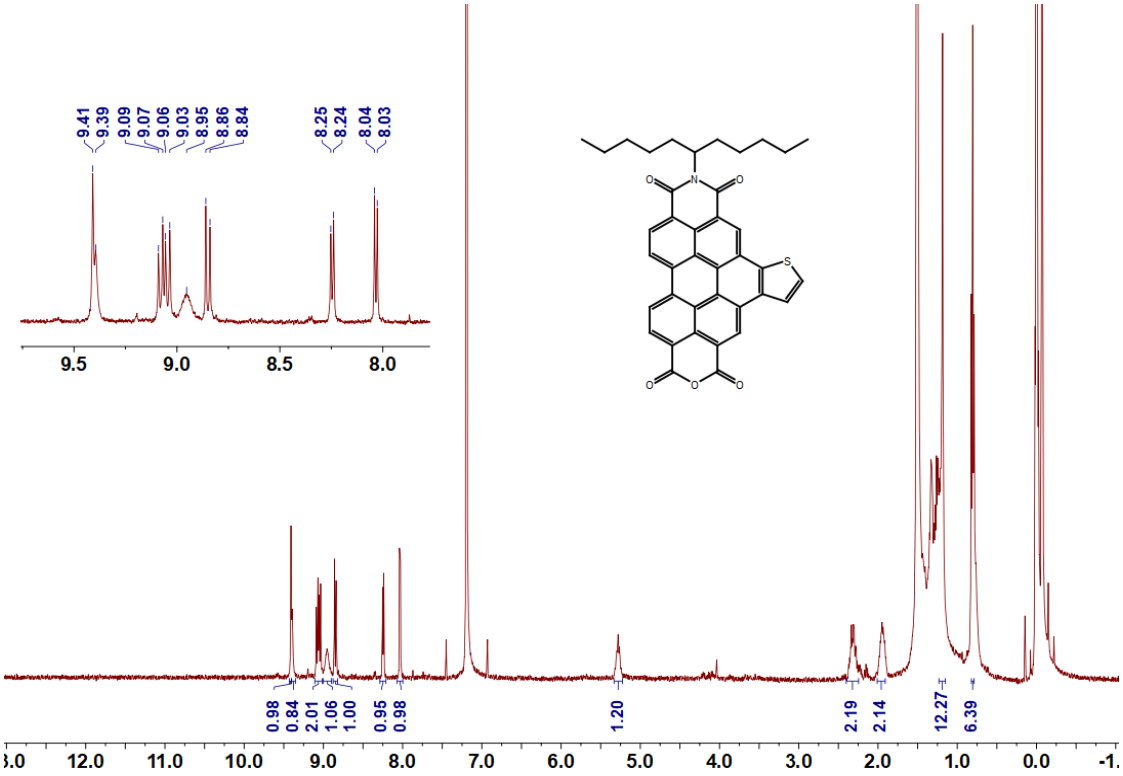

Figure S24. ^{1}H NMR spectrum of ThPMA (400 MHz, $CDCl_3$).

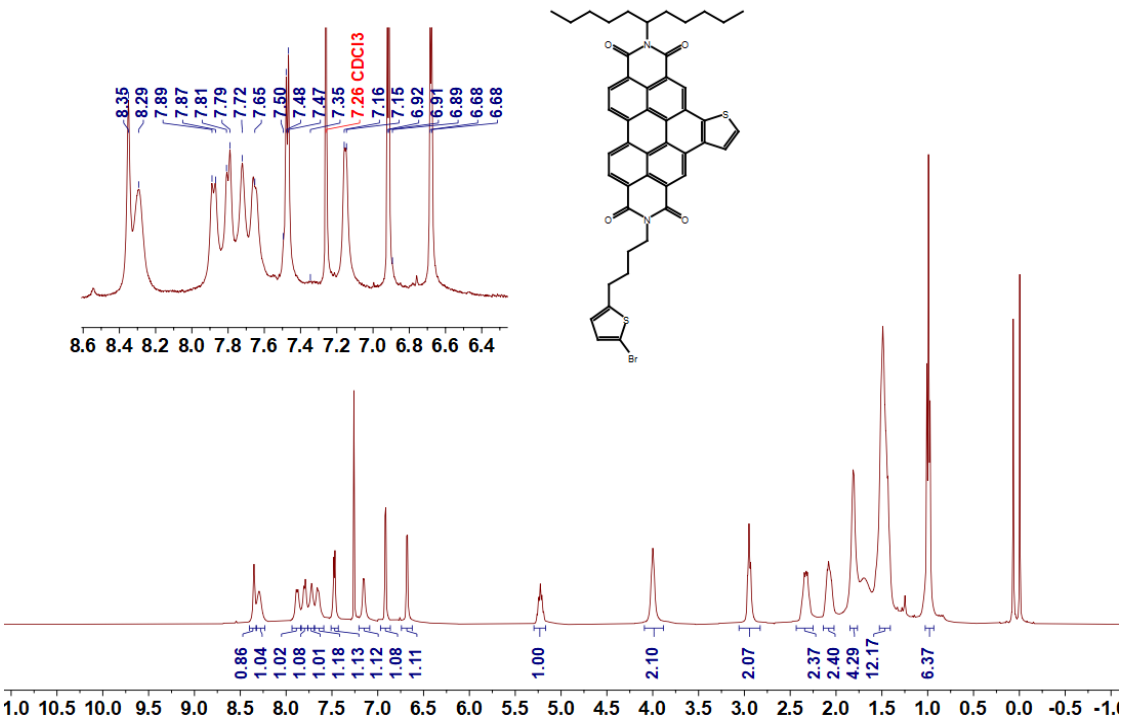

Figure S25. ^{1}H NMR spectrum of M-Br-4 (400 MHz, $CDCl_3$).

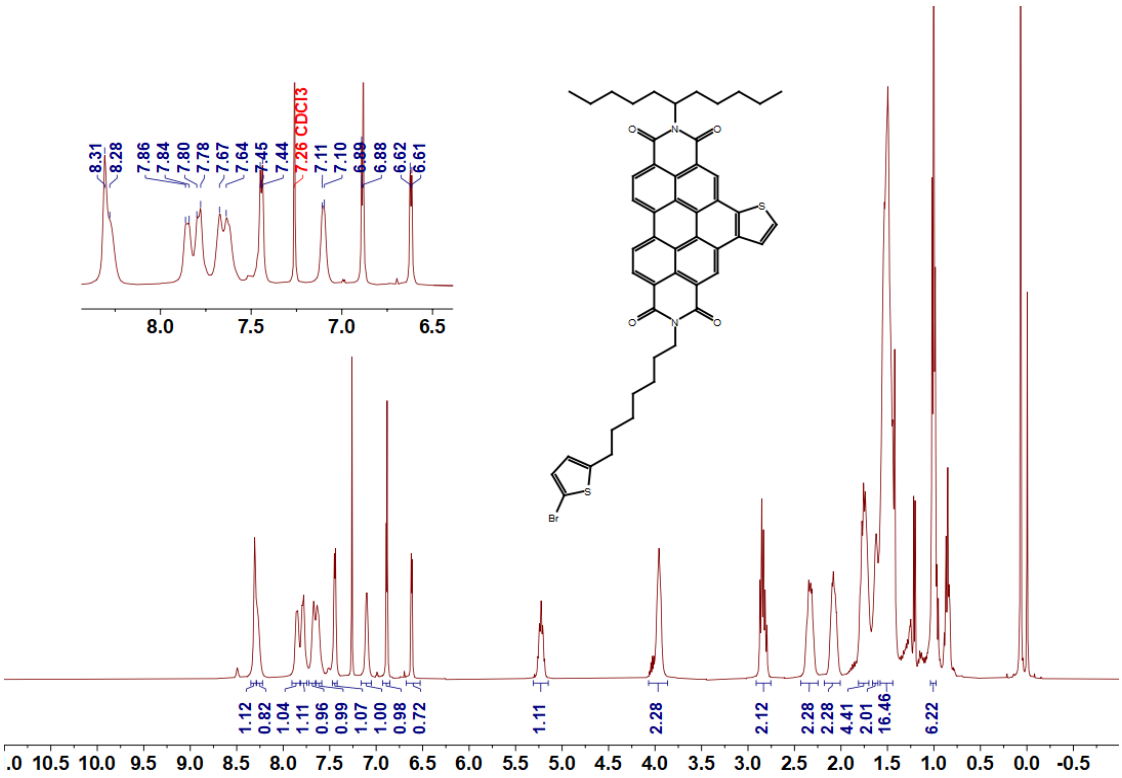

Figure S26. ^{1}H NMR spectrum of M-Br-7 (400 MHz, $CDCl_3$).

10. References

1 P. Pigeon and B. Decroix, *J. Heterocycl. Chem.*, 1996, **33**, 129–135.

2 N. Cernetic, T. Weidner, J. E. Baio, H. Lu, H. Ma and A. K.Y. Jen, *Adv. Funct. Mater.*, 2015, **25**, 5376–5383.

3 D. Meng, H. Fu, C. Xiao, X. Meng, T. Winands, W. Ma, W. Wei, B. Fan, L. Huo, N. L. Doltsinis, Y. Li, Y. Sun and Z. Wang, *J. Am. Chem. Soc.*, 2016, **138**, 10184–10190.

4 R. Wang, Z. Shi, C. Zhang, A. Zhang, J. Chen, W. Guo and Z. Sun, *Dyes Pigm.*, 2013, **98**, 450–458.

5 M. E. Madjet, A. Abdurahman and T. Renger, *J. Phys. Chem. B*, 2006, **110**, 17268–17281.

6 H. Yamagata, D. S. Maxwell, J. Fan, K. R. Kittilstved, A. L. Briseno, M. D. Barnes and F. C. Spano, *J. Phys. Chem. C*, 2014, **118**, 28842–28854.

7 X.Y. Li, X.S. Tang and F.C. He, *Chem. Phys.*, 1999, **248**, 137–146.

8 G. Bressan, S. E. Penty, D. Green, I. A. Heisler, G. A. Jones, T. A. Barendt and S. R. Meech, *Angew. Chem. Int. Ed.*, 2024, **63**, e202407242.

9 Z. Chen, V. Stepanenko, V. Dehm, P. Prins, L. D. A. Siebbeles, J. Seibt, P. Marquetand, V. Engel and F. Würthner, *Chem. Eur. J.*, 2007, **13**, 436–449.

10 J. Hofkens, T. Vosch, M. Maus, F. Köhn, M. Cotlet, T. Weil, A. Herrmann, K. Müllen and F. C. De Schryver, *Chem. Phys. Lett.*, 2001, **333**, 255–263.

11 Z. Lou, Y. Hou, K. Chen, J. Zhao, S. Ji, F. Zhong, Y. Dede and B. Dick, *J. Phys. Chem. C*, 2018, **122**, 185–193.

12 S. M. King, C. Rothe, D. Dai and A. P. Monkman, *J. Chem. Phys.*, 2006, **124**, 234903.